SNOW AVALANCHES: HAZARD MAPS AND
PASSIVE DEFENCE STRUCTURES

FRANCESCA MORO

Dipartimento di Geoscienze, Università di Padova, Via Giotto 1, 35137 Padova

ABSTRACT

In Alpine regions snow avalanches are a severe threat for human settlements, activities, and infrastructures.

Such natural phenomena may be of two types: powder and dense snow avalanches. The countermeasures against powder avalanches consist in preventing the motion initiation by means of active structures built in the detachment area, or in artificial triggering of avalanche events in controlled conditions or at least in no-risk conditions. Passive defence structures along the path and in the run-out zone can instead be very effective in deflecting, retarding, or stopping dense snow avalanches. Nevertheless this kind of works is much of less used and not completely understood.

In this thesis some aspects of dense snow avalanches have been experimentally investigated using a granular mass. Small-scale laboratory tests have been performed to study the different types of deposit that dense snow avalanches can form and to measure the impact force on retarding structures located along the run-out zone.

A procedure for the estimation of dense snow avalanches hazard maps has been defined and the effects of the main physical parameters have been analysed.

INTRODUCTION

Significant field evidences prove that dense snow avalanches, after a first phase of granulation, move downstream and stop in almost the same way as granular materials (Fig. 1).

Recent detailed measurements (Rognon *et al.*, 2008), made in a large scale channel using real snow, highlight a thin layer -just above the base- composed of granular snow, as a result of granulation. Most of the velocity occurs in this layer whilst the upper mass moves almost undisturbed.

Due to the above observations dense snow avalanches are often modelled adopting small-scale

Fig. 1 - Example of granular deposit of an avalanche occurred in Val di Levi (Trentino Province, Italy).

laboratory experiments, using dry granular materials that flow down an inclined plane. Many small-scale (Norem & Brateng, 2005; Sheikh *et al.*, 2008) and large-scale laboratory tests (Hákonardóttir *et al.*, 2003; Faug *et al.*, 2008) on snow avalanches shown a significant dissipation of the flow energy if retarding structures are introduced in the motion field. In particular, the impact force has been investigated to define project parameters (see, *e.g.*, Favier & Daudon, 2006; Kulibaba & Eglit, 2008).

So far the design of passive defence structures has been mainly empirical and based on the personal experience of technicians. The problem can be faced studying the effect of the use of retarding elements in terms of energy dissipation of the moving mass and analysing the impact against the same retarding elements. This second point of view has been adopted in this research.

EXPERIMENTAL ANALYSIS ON THE CHARACTERIZATION OF AVALANCHE DEPOSITS

In order to analyse the influence of grain size distribution of the granular material mixture that simulates dense snow avalanches, experimental investigation was carried out at the Avalanche Laboratory of the Cemagref de Grenoble in France.

The tests consisted in releasing, from a feeding-box, a mass of glass beads that first flowed down along an inclined channel and finally spread out on an inclined unconfined deposition zone (Fig. 2). The mass ratio (r) between fine grains (150-250 μm size) and large grains (~ 1 mm), in the released mass, was systematically changed to determine its influence on: i) the incoming flow depth and front velocity in the channel, measured by a laser line technique; ii) the shape of the deposited mass, measured by an accurate fringe analysis technique.
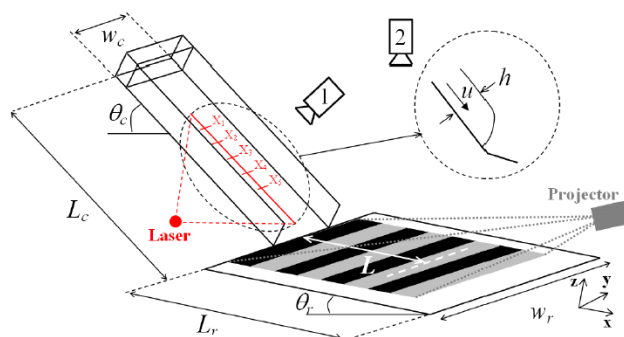

Fig. 2 - Sketch of the experimental set-up and instrumentation. The channel width (w_c) was 0.30 m, its length (L_c) was 1.50 m and its slope inclination (θ_c) was 35°. The width of the downstream plane (w_r) was 1.20 m, its length (L_r) 2.50 m and its slope inclination (θ_r) was 6° (Laboratory of the Cemagref de Grenoble, France).

In particular, in each experimental test a mass of 10 kg was released, and the r was changed at each test, ranging from to 0 to 65% with a 1% step. Moreover, tests with r values of 80% and 100% were carried out.

The laser line technique

A laser light plane is generated and it is projected along the longitudinal axis of the channel, forming a line of light with the inclined plane (Fig. 2). When the granular mass propagates on the channel, this laser line is deflected. Thanks to a video-camera placed normal to the channel bottom, it is possible to visualize the shifted laser line. In particular, the zone acquired by the video-camera has a length of 1 m, corresponding to the zone between the locations x_1 and x_5 (Fig. 2). The deviation is directly

proportional to the flow thickness. A calibration phase, carried out by using several rectangular objects of known thickness allows the computation of the proportionality coefficient. In this way, the thickness at each time t and at each point x (in the center of the channel) can be easily derived.

The precision of depth measurements has been estimated to 1 mm. Moreover, the dynamic observation of the laser line allows the recognition of the front motion x in the channel and, consequently, leads to the propagation velocity of the granular front. The corresponding precision was estimated to 0.1 m s^{-1}.

The fringe analysis technique

Parallel fringes, alternatively black and white, were projected on the granular mass on the run-out zone by a projector (Fig. 2). Like the shifted laser line, the fringes network is shifted by the granular mass and the deviation is proportional to the deposit thickness. A video-camera placed normal to the inclined plane allows the visualization of the shifted fringes network.

The key factor of the fringe analysis technique is an accurate evaluation of the phase difference $\Delta\varphi(x,y)$ between the *reference* signal, without the granular mass, and the *object* signal, in presence of the granular mass which distorts the fringes. Here, x is the coordinate along the lower plane axis and y is the transverse coordinate (Fig. 2). The *reference* signal is modelled by a sinusoidal waveform:

$$I_{\text{ref}}(x,y) = \bar{I}(x,y) + \bar{I}(x,y)\,\gamma(x,y)\cos(\varphi_0 + 2\pi f_0 x) \tag{1}$$

where $\bar{I}(x,y)$ is the mean intensity of the signal, $\gamma(x,y)$ the lightness contrast at the point (x,y), f_0 is the frequency linked to interfringe and φ_0 the origin phase. The object signal is instead:

$$I_{\text{object}}(x,y) = \bar{I}(x,y) + \bar{I}(x,y)\,\gamma(x,y)\cos[\varphi_0 + 2\pi f_0 x + \Delta\varphi(x,y)] \tag{2}$$

where the phase difference $\Delta\varphi(x,y)$ between the two signals is directly proportional to the local deviation of fringes $\delta(x,y)$, *i.e.*

$$\Delta\varphi(x,y) = 2\pi f_0\,\delta(x,y) \tag{3}$$

An empirical calibration was carried out by using rectangular objects of known height to deduce the deposit thickness at each point (x,y) of the inclined plane.

Several methods have been proposed in order to evaluate the phase difference (see, *e.g.*, Surrel, 1993; Vincent, 2003). For example, a single image projection of the fringes network is carried our together with a Fourier transform. More accurate methods are instead based on the principle of phase shifting, where several images shifted one to each other are projected. In the experiments presented here, the phase shifting was the chosen method and four grids shifted of $\pi/2$ were projected. In particular, the displacement of fringes due to the granular mass was interpreted as a fringes phase modulation and was computed from the four intensities $I_i(x)$ according to:

$$\varphi(\text{x}) = \arctan[I_4(x) - I_2(x)] / [I_1(x) - I_3(x)] \tag{4}$$

where the four shifted images ($\varphi_1 = 0$, $\varphi_1 = \pi/2$, $\varphi_1 = \pi$, $\varphi_1 = 3\pi/2$) have sinusoidal waveform:

$$I_i(x,y) = \bar{I}_i(x,y) + \bar{I}_i(x,y)\,\gamma(x,y)\cos[\varphi(x) + \Delta\varphi_i(x)] \tag{5}$$

The thickness was then obtained from the phase modulation $\varphi(x)$. The calibration procedure was performed by projecting the four *reference* shifted images ($\varphi_1 = 0$, $\varphi_1 = \pi/2$, $\varphi_1 = \pi$, $\varphi_1 = 3\pi/2$) on various

rectangular objects of known height. The precision varied according to the image quality and was generally smaller than 500 μm.

Experimental results

The experimental results showed that the main dynamic characteristics of the granular flow are strongly influenced by the ratio between the mass of fine and large particles. In particular, the fact that the front velocity increased when some fine material was added up until a *r* equal to the 30%, while such velocity remained constant afterwards, was observed. The maximum flow depth decreased of roughly 10% when the *r* was above 30%. The maximum stopping distance increased of about 30% at the 25% *r* (Fig. 3). An important diameter segregation was observed in the deposit.
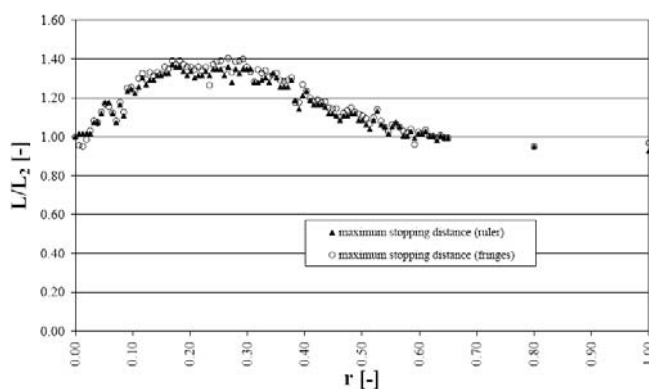

Fig. 3 - Stopping distance of the deposit (*L*) normalized by the stopping distance of the deposit (*L₂*) obtained with the large grains of diameter only versus the mass ratio in fine particles (*r*). Results from the fringes projection technique (white circles) as well as from the direct measurements with a ruler (black triangles) are shown.

PASSIVE DEFENCE STRUCTURES: EXPERIMENTAL ANALYSIS ON RETARDING MOUNDS

In order to analyse the behaviour of some defence structures used in the practice of environmental engineering to slow down dense snow avalanches, an experimental investigation was performed at the Hydraulic Laboratory of the University of Trento in Italy.

Retarding cone-shaped and tooth-shaped structures, organized in a system of three elements arranged in two lines, were used. The tests were performed in a flume using granular zeolite as flowing material (average diameter of about 1 mm). The experimental set-up of the physical model can simulate real phenomena following the Froude similarity with a geometrical scale of about 1/100.

About 130 experiment runs were performed and the corresponding data analysed. The lower plane inclination was held at 7°. The upper plane inclinations were 24°, 27° and 30° (Fig. 4). Two masses were chosen for the whole falling material, *i.e.* 3 kg and 7 kg.

The measurements of impact force

Two types of load cells were used to perform the laboratory experiments: Futek model L1510 (protected) and Futek model L1501 (not protected). Data acquisition was performed using Spider8-HBM which is a multi-channel electronic PC measurement unit for parallel, dynamic measurement data acquisition. Before the implementation of each test, the force measurement system was calibrated.
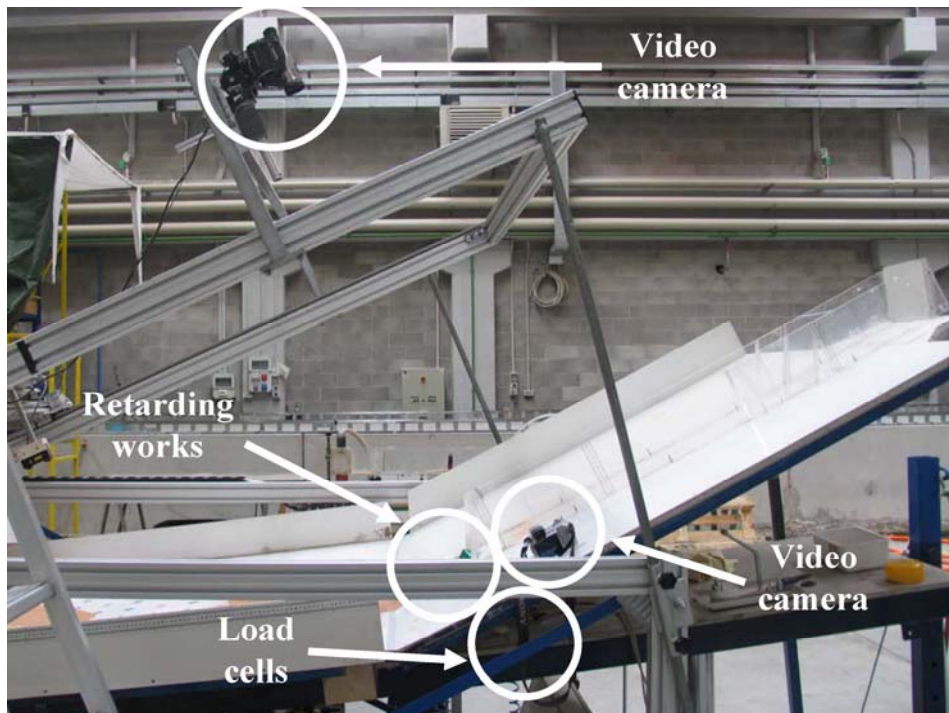
Fig. 4 - The experimental chute with the instrumentation. The channel width was 0.20 m, its length was 1.50 m and its slope inclination was 24°-27°-30°. The width of the downstream plane was 1.50 m, its length 1.50 m and its slope inclination was 7° (Laboratory of the University of Trento, Italy).

The dimensionless impact force was computed from the zeolite density ($\rho = 1080$ kg/m^3), the velocity of the mixture flow near to the simulated retarding works (v) and the impact area (A) according to:

$$F_{d\_less} = F / [\rho \, v^2 \, A] \tag{6}$$

The values of the force against the front element ranged from 0.64 to 2.84 N, while against the rear elements from 0.16 to 2.26 N.

The measurements of flow velocity, flow depth and mixture spreading

The measurement of flow velocity and flow depth was carried out by means of two digital video-cameras. A video-camera was placed above the upper plane, to cover the area between the end of the chute and the slowing down elements. The second video-camera was placed laterally to the final part of the chute in order to shoot the flowing depth of the mixture at a section very near to the works.

The final longitudinal and cross-sectional mixture spreading were obtained by image processing. Mixture spreading depends on type of works (circular base cones, elliptical base cones and tooth-shaped works) and on the respective position of the elements. The rear line of works was located at a longitudinal distance from the upstream element of about twice the height of the works (70 mm). The rear element was

located at various positions along the cross-sectional guide. The angle, between the longitudinal flow direction and the line passing through the front and the rear element, ranged from 26° to 45°.

In order to characterize the mixture spreading, two physical parameters were computed: the longitudinal efficiency and the cross-sectional efficiency. The cross-sectional efficiency was obtained by:

$$\varepsilon_T = [L - L_{NW}] / L_{NW} \tag{7}$$

where L is the deposit width and L_{NW} is the maximum width of the mixture at rest in the case of absence of slowing down elements. The longitudinal efficiency was computed as follows:

$$\varepsilon_L = [d_{NW} - d] / d_{NW} \tag{8}$$

where d is the deposit stopping distance and d_{NW} is the maximum distance travelled by the mixture in the case of absence of slowing down elements (Fig. 5).
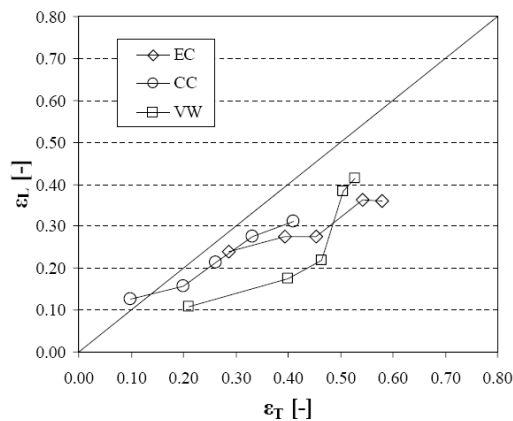

Fig. 5 - Relationship between mean values of cross-sectional efficiency (ε_T) and longitudinal efficiency (ε_L) for the various type of retarding structures systems for the three different type of structures.

Experimental results

The experimental analysis proved that: i) the dimensionless force is much bigger for systems that use tooth-shaped elements instead of cone-shaped structures; ii) the opening angle of the rear elements at which the cross-sectional and the longitudinal efficiency present their maximum value is around 26° and that maximum efficiency occurs when the dimensionless force is at its maximum. The phenomena produced in the laboratory can be thought to represent real phenomena in the Froude similarity at a scale in the order of magnitude of roughly 1/100. Confirmation of the experimental results should be given at a higher scale.

THE SPINI VALLEY AVALANCHE SITE

Avalanche zoning plans are usually the result of government decisions (Barbolini *et al.*, 2005). Normally, in Italy, the hazard zone is divided into three areas with respect to a return period T_r: a red area (T_r = 30 years), a blue area (T_r = 100 years), and a yellow area (T_r = 300 years). The different areas are defined by the conjunction of the points representing the stopping distances, along different trajectories, that the mass can travel for the same return period.

The FLO-2D™ model, a 2-D commercial numerical model, was tested with the aim to define a hazard map of the Spini Valley (Trento Province) avalanche site, located in the north-eastern part of Italy

(Fig. 6). The necessary physical parameters were calibrated by means of two real events and a comparison with the hazard maps already realized with a 1-D model (Scotton *et al.*, 2006), based on the rheology of Savage & Hutter (1989), was carried out.
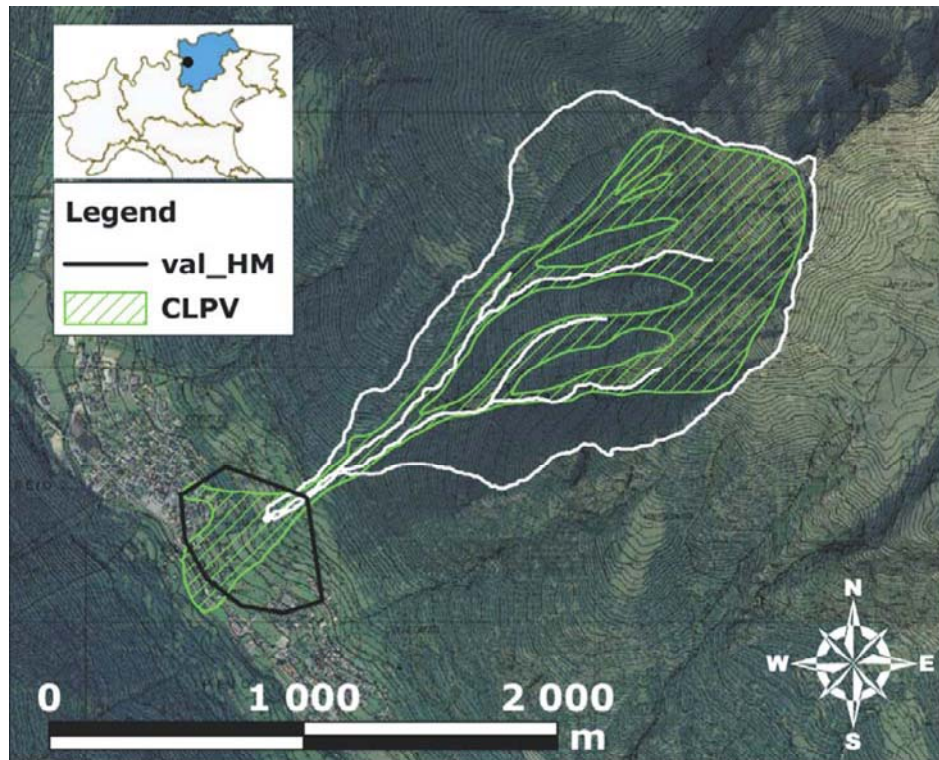

Fig. 6 - The Spini Valley (Trento Province, Italy) avalanche site with the main flow channels; the avalanche hazard map for the channel 1 for the return period of 100 years (val_HM, Scotton *et al.*, 2006) and the CLPV (avalanche probable localisation map).

A sensitivity analysis was performed to show the effects on the hazard map of the physical and topographical parameters of the simulations. In the present application the dominant rheological parameters of FLO-2D™ model were the Manning coefficient and the yield stress. Their values were changed in a quite wide range also beyond the range indicated in the available literature (Dent & Lang, 1982).

A strong influence of the boundary conditions was observed, in particular depending on the shape of the input hydrograph. As a consequence, a reliable hazard map of the site cannot be obtained on the basis of this particular code.

The most important limitations on application of the model are: i) the uncertain physical meaning of the rheological parameters: to obtain a good simulation of some parameters of the calibration events it was necessary to assign values quite far from those suggested in the available literature; ii) the calculation time and numerical stability. Under many initial and boundary conditions (large avalanche volumes and small grid cell size) it was practically impossible to obtain a reliable solution.

A procedure for the determination of the snow avalanches hazard maps was sketched and the physical parameters of the numerical-mathematical model were calibrated on the basis of the knowledge of two real events.

CONCLUSIONS

The main aim of all the researches performed in this topic -from an engineering point of view- is to produce maps that allow proper land management (hazard maps, risks maps). This research analyses some relevant aspects of the behaviour of granular fluxes which represent dense snow avalanches. The two performed experimental campaigns describe some aspects of the interaction between the size distribution of the granular mass and the dynamic characteristics of the motion and the interaction with retarding structures.

The first experiments show that the main characteristics of the deposits are strongly influenced by the ratio between fine and large particles; in particular the maximum stopping distance corresponds to a poorly sorted material composition. The experimental results highlight that the size distribution of granular material is a key factor that must be taken into account in experimental investigations aimed at calibrating physical parameters of numerical models. This fact could have a considerable effect on the definition of physical parameters used in the construction of hazard maps.

The second experimental investigation gives some technical information that can be used in the design process of retarding structures aimed to reduce stopping distance and to favour the spread of the flowing mass. The experimental results can be used in order to test the capability of numerical models to simulate the impact against retarding structures. This aspect assumes particular importance when the residual hazard map is to be evaluated as a consequence of the introduction of retarding structures in the motion field.

REFERENCES

Barbolini, M., Natale, L., Tecilla, G., Cordola, M. (2005): Linee guida metodologiche per la perimetrazione delle aree esposte al pericolo valanghe. Dipartimento di Ingegneria Idraulica e Ambientale dell'Università degli Studi di Pavia, AINEVA, 164 p.

Dent, J.D. & Lang, T.E. (1982): Experiments on the mechanics of flowing snow. *Cold Reg. Sci. Technol.*, **5**, 253-258.

Faug, T., Gauer, P., Lied, K., Naaim, M. (2008): Overrun length of avalanches overtopping catching dams: cross-comparison of small-scale laboratory experiments and observations from full-scale avalanches. *J. Geophys. Res.*, **113**, F03009.

Favier, L. & Daudon, D. (2006): Impact forces of dense granular flow against an obstacle. *In*: "Annual Report 2006 - Discrete Element Group for Hazard Mitigation 3S-R", F.V. Donzé, ed. Université Joseph Fourier, Grenoble, France, H1-H8.

Hákonardóttir, K.M., Hogg, A.J., Jóhannesson, T., Kern, M., Tiefenbacher, F. (2003). Large-scale avalanche braking mound and catching dam experiments with snow: a study of the airborne jet. *Surv. Geophys.*, **24**, 543-554.

Kulibaba, V.S. & Eglit, M.E. (2008): Numerical modeling of an avalanche impact against an obstacle with account of snow compressibility. *Ann. Glaciol.*, **49**, 27-32.

Norem, H. & Brateng, L.E. (2005): Effect of dams and mounds to retain snow avalanches. *In*: "Landslide and avalanches", K. Senneset, K. Flaate & J.O. Larsen, eds. Taylor and Francis Group, London, 279-285.

Rognon, P., Chevoir, F., Bellot, H., Ousset, F., Naaim, M., Coussot, P. (2008): Rheology of dense snow flows: inferences from steady state chute-flow experiments. *J. Rheol.*, **52**, 729-748.

Savage, S.B. & Hutter, K. (1989): The motion of a finite mass of granular material down a rough incline. *J. Fluid Mech.*, **199**, 177-215.

Scotton, P., De Toni, S., Sebastiani, M. (2006): Studio del sito valanghivo della Val dei Spini. Technical Report. Department of Civil and Environmental Engineering, University of Trento, 70 p.

Sheikh, A.H., Verma, S.C., Kumar, A. (2008): Interaction of retarding structures with simulated avalanches in snow chute. *Current Sci.*, **94**, 916-921.

Surrel, Y. (1993): Phase stepping: a new self-calibrating algorithm. *Appl. Opt.*, **32**, 3598-3600.

Vincent, C. (2003): Recalage et fusion pour reconstruire de surfaces 3D obtenues par projection de franges. Application à un système de vision dédié à l'orthopédie. Thèse, Université Jean Monnet, Saint-Étienne.